where $C_{ROI}(t)$ and $C_b(t)$ are the measured radioactivity concentrations of the region and total blood, respectively. Each kinetic parameter, including V_b, was estimated by nonlinear least-squares fitting procedure without weighing. For the cerebellum, the 1-tissue model was also applied. The appropriate model of the cerebellum was evaluated by the Akaike information criterion [28].

Plasma-input Logan analysis

The total distribution volume was calculated by plasma-input Logan analysis developed by Logan et al. [29]. After an equilibrium time (t^*), the following linear relationship is obtained:

$$\frac{\int_0^t C_T(s)ds}{C_T(t)} = a\frac{\int_0^t C_p(s)ds}{C_T(t)} + b \quad (t > t^*), \tag{10}$$

where the slope a denotes the total distribution volume. In this analysis, t^* was determined so that the maximum discrepancy from the regression line within the linear segment would be 10% for each time–activity curve (TAC). To test the possible underestimation of striatal V_T generated by too early t^*, the caudate TAC of the earliest t^* was re-estimated with fixed t^* at the latest one.

Quantification using reference tissue data without arterial input function

To avoid measurements of arterial input function, noninvasive analysis employing a reference region with negligible specific binding was applied. *DVR* is derived from the TACs of the brain regions and reference region. In the case of DAT, the cerebellum was reported not to express any mRNA [30]. Pretreatment and blocking studies of [^{11}C]PE2I in monkeys showed no changes in cerebellar TACs [11]. Therefore, the cerebellum was used as a reference brain region. In this study, MRTMo and SRTM were applied to calculate *DVR*.

MRTMo method

MRTMo is one of the variations of the graphical approach. After a certain equilibrium time (t^*), the following multilinear regression is obtained:

$$\frac{\int_0^t C_t(s)ds}{C_t(t)} = \frac{a}{a'}\frac{\int_0^t C_{ref}(s)ds}{C_t(t)} + \left(-\frac{ab'}{a'}\right)\frac{C_{ref}(t)}{C_t(t)} + b, \tag{11}$$

where C_t and C_{ref} are tissue radioactive concentrations of the target brain and reference regions, respectively, a and a' are the distribution volumes of the target brain and the reference regions, respectively, and therefore a/a' denotes *DVR*. b' and b are $-1/k_2'$ and $-1/k_2$, respectively, where k_2' is k_2 of the reference region. The time t^* was determined in the same way as described in the plasma-input Logan analysis previously.

SRTM method

In the SRTM method, *DVR* can be determined by modification of the original SRTM equation as follows:

$$C_t(t) = R_1 C_{ref}(t) + \left(R_1 k_2' - R_1\frac{R_1 k_2'}{DVR}\right) C_{ref}(t) \otimes \exp\left(-\frac{R_1 k_2'}{DVR}t\right), \tag{12}$$

where R_1 is K_1/K_1' and K_1' is K_1 of the reference tissue. *DVR* is calculated by the non-linear least-squares fitting procedure.

All of the analysis described above was performed with PMOD Ver. 2.6 (PMOD Technologies, Zürich, Switzerland).

Preparation of [^{11}C]PE2I

[^{11}C]PE2I was synthesized by *O*-methylation of the corresponding precursors with [^{11}C] methyl iodide with ultra-high specific activity, which was obtained by a reduction of [^{11}C]CO_2 with $LiAlH_4$ in an inert atmosphere with specially designed equipment [31], and automatically purified [32].

Subjects

Six healthy male volunteers (age 20–28 years, 23.8 ± 3.1, mean ± SD) participated in this study. All subjects underwent 1.5 T T1-weighted MRI examinations to obtain anatomical brain references for the PET images. The MRI scanner was Intella (Philips Medical Systems, Best, The Netherlands). Three-dimensional volumetric acquisition of a T1-weighted gradient echo sequence produced a gapless series of thin transverse sections (TE: 9.2 ms; TR: 21 ms; flip angle: 30°; field of view: 256 mm, acquisition matrix: 256 × 256; slice thickness: 1 mm). None of the subjects had a significant medical history or brain morphological abnormalities. This study was performed in compliance with the Declaration of Helsinki and approved by the Ethics and Radiation Safety Committees of the National Institute of Radiological Sciences, Chiba, Japan. Written informed consent was obtained from all subjects prior to the study.

PET measurement

PET data were acquired using an ECAT EXACT HR+ (CTI-Siemens, Knoxville, TN, USA) in 3-dimensional

mode, which provides 63 sections with an axial field of view of 15.5 cm [33]. The intrinsic in-plane and axial resolutions were 4.3 and 4.2 mm full width at half maximum (FWHM), respectively. The dynamic PET image data were corrected for physical decay of ^{11}C. An individualized thermal plaster mouthpiece and nose plate were used for head immobilization during the PET scanning. A cannula was inserted into the brachial artery for arterial blood sampling. Prior to the emission scan, a 10-min transmission scan was performed using a ^{68}Ge–^{68}Ga rod source. After intravenous rapid bolus injection of [^{11}C]PE2I, a 90-min dynamic PET scan was performed (35 frames: 9 × 20 s, 5 × 1 min, 4 × 2 min, 12 × 4 min, 5 × 6 min). The injected dose and specific radioactivity were 197–230 MBq and 644–1104 GBq/μmol at the time of injection, respectively. The emission data were reconstructed with a Hanning filter (cutoff frequency: 0.4 cycle/pixel), and the reconstructed in-plane resolution was 7.5 mm FWHM.

Arterial input function

Frequent arterial blood sampling was performed throughout the scan. For the first 5 min after the injection, arterial blood was withdrawn using a peristaltic pump at a constant rate to monitor whole blood radioactivity with an automatic radioactive monitoring system [34] simultaneously with blood sampling at the end of the tube. The sampling time points after the tracer injection were as follows: every 10 s from 15 to 105 s, then 120, 150, 180 s and every 1 min from 4 to 6 min, every 2 min from 6 to 12 min, 15, 20 min and every 10 min from 20 to 90 min. The radioactivity in each sample was measured with a well-type auto-gamma counter (COBRA II Auto Gamma, Packard Instrument Co., Meriden, CT, USA) to obtain the radioactive concentration in whole blood. Then the blood samples were centrifuged, and an aliquot of plasma was taken to measure the total radioactive concentration in plasma. The sensitivities of the continuous monitoring system and well-type gamma counter were cross-calibrated with that of the PET system.

Radioactive fractions of unmetabolized [^{11}C]PE2I in plasma were evaluated by HPLC radiochromatography. Arterial blood samples taken at 3.5 min and every 10 min from 9 to 89 min after the tracer injection were centrifuged and a 1-mL aliquot of plasma was added with the same amount of acetonitrile. The mixture was vortexed and centrifuged at 13000 rpm for 2 min with a refrigerated centrifuge. Then an aliquot of 0.5 mL of the supernatant was injected into the HPLC system (GL Sciences Inc., Tokyo, Japan). The analytical column was Waters μBondapak C18 (300 × 7.5 mm i.d.), the mobile phase was acetonitrile and 0.1 M ammonium formate (70/30) at an isocratic condition, and the flow rate was 6.0 mL/min. The radiochromatography peak of [^{11}C]PE2I was identified by standard PE2I at the detection wavelength of 254 nm. The unchanged fraction was calculated as the peak area ratio of unchanged [^{11}C]PE2I to the total peaks detected. The time course of unchanged [^{11}C]PE2I fraction was approximated by a power function ($y(t) = At^{-b}$; $y(t) = 1$ when $At^{-b} > 1$ during the first few minutes) individually. The arterial input function was obtained as the product of plasma radioactive concentration and the unchanged fraction. The time lag between brain TACs and input function was adjusted at their onsets individually. Plasma protein binding was not determined in the present study.

Regions of interest

T1-weighted MRI images were coregistered and resliced to PET images using SPM2 [35]. Polygonal regions of interest (ROIs) were drawn on the MRI images and placed on the PET summation images. The regions chosen in this study were the cerebellum, pons, temporal cortex, frontal cortex, occipital cortex, parietal cortex, caudate head, thalamus, putamen, midbrain, parahippocampal gyrus, anterior part of the cingulate gyrus, and white matter (central semiovale). Then the ROIs were placed on the dynamic PET images to obtain regional TACs. The TACs were corrected for physical decay of ^{11}C.

Simulation study

To estimate errors in *DVR* calculated by the reference tissue models for [^{11}C]PE2I kinetics in human brain, a simulation study was performed. Brain TACs were generated using assumed kinetic parameters taken from the results of the kinetic analysis of [^{11}C]PE2I. For the reference region, kinetic parameters were assumed for both 1- and 2-tissue models. Kinetic parameters of the reference region were set as $K_1' = 0.25$, $K_1'/k_2' = 2$, $k_3' = 0.0089$ and $k_4' = 0.019$ for the 2-tissue model, and $K_1' = 0.25$ and $K_1'/k_2' = 2$ for the 1-tissue model. The simulation results when the reference tissue kinetics as the 1-tissue model at $K_1'/k_2' = 2.45$ was similar to those of $K_1'/k_2' = 2.0$ (data not shown). To highlight the contribution of the second tissue compartment of the reference region, a uniform K_1'/k_2' value was applied. Also, despite the fact that the K_1/k_2 values of striatal regions were approximately fivefold higher than those of other regions, K_1/k_2 and k_4 of the target brain region parameters were assumed to be the same values as the reference region parameters. The result of the preliminary simulation using $K_1/k_2 = 10$ was similar to that of $K_1/k_2 = 2.0$ (data not shown). K_1 of the target region was fixed at 0.20 and k_3 was varied to alter *DVR*. The range of k_3 was from 0.0005 to 0.35 in 26 steps or 0.01–0.55 in 24 steps when the reference tissue kinetics was for the 1-tissue or 2-tissue model, respectively, to

cover the *DVR* range from 1.03 to 20. The fractional blood volume (V_b) was fixed at 0.04 mL/mL for all conditions. A typical metabolite-corrected input function and whole blood TAC were used to generate TACs. The assumed *DVR* was determined as the ratio of V_T calculated by Eq. 7 of the target brain region to that of the reference region. For each simulated TAC, *DVR* was estimated by MRTMo and SRTM and compared to the corresponding assumed *DVR* value. Another simulation was performed to test whether the scan duration of 90 min was sufficient when the reference region kinetics was according to the 2-tissue model.

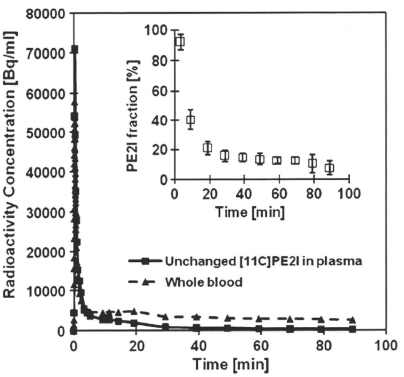

Fig. 1 Arterial input function. Typical time–activity curves of arterial whole blood (*filled triangles*) and unchanged [^{11}C]PE2I in plasma (*filled circles*). The *inset* is the mean fraction of unchanged [^{11}C]PE2I in plasma obtained from the 6 subjects. The *error bars* indicate 1 standard deviation

The input function was exponentially extrapolated with a single exponential to 240 min (4 h) using 30–90-min data, and 4-h target tissue curves were generated in the same manner as described above. Then, *DVR* was estimated by MRTMo and SRTM. For MRTMo, in addition to the determination of t^* as the time when the percentage deviation from the model was within 10% for each case, *DVR* was calculated when t^* was fixed at 120 min for all cases.

Results

Input function

Figure 1 shows the typical time course of the radioactive concentration of whole blood and that of unchanged [^{11}C]PE2I in plasma. The average time course of the unchanged fraction is also shown. The metabolism of [^{11}C]PE2I is relatively fast, and so the unchanged [^{11}C]PE2I fraction was 25% at 20 min after injection and continued to decline gradually until the end of the scan.

PET images and ROIs

A typical example of PET images of [^{11}C]PE2I obtained by summation of the frames from 0 to 90 min after injection and coregistered T1-weighted MRI images is shown in Fig. 2. Higher radioactivity concentrations were observed in the caudate head and putamen, regions known to be rich in DAT. Among other regions, the midbrain and thalamus showed some [^{11}C]PE2I binding, whereas the cerebellum and other cortical regions demonstrated very little.

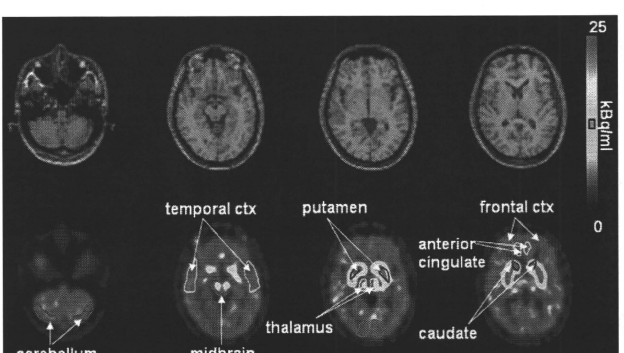

Fig. 2 Coregistered T1-weighted MRI images and [^{11}C]PE2I images (summed image of 0–90 min) with ROIs

Brain TACs

Typical TACs of various cerebral regions are shown in Fig. 3. Marked [^{11}C]PE2I uptake and retention are observed in the putamen. Midbrain and thalamus showed slower clearance than the cerebellum and other cortical regions, and radioactivity concentrations in the midbrain and thalamus were higher than in other regions at the end of the scan, with the lowest observed in the cerebellum. The TAC of the putamen reached a plateau within 90 min after the injection in all subjects, indicating the reversibility of this tracer. In other regions, TACs attained peaks a few minutes after the injection and then declined faster than that of the putamen.

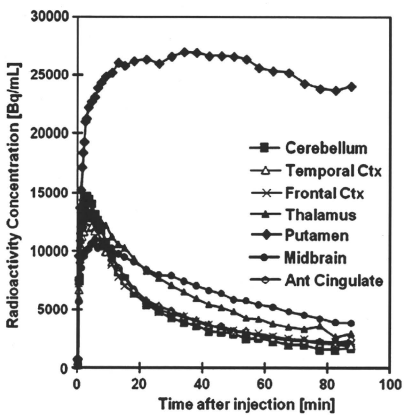

Fig. 3 Typical time–activity curves of [^{11}C]PE2I in the human brain

Kinetic analysis and plasma-input Logan analysis

TACs of all ROIs were well described by the 2-tissue model. Table 1 shows the mean kinetic parameters obtained by kinetic analysis with 2-tissue model analysis. For the cerebellum, kinetic analysis with the 1-tissue model was also applied. Figure 4 shows a cerebellar TAC and the fitted curves with 1- and 2-tissue models, respectively. The mean kinetic parameters of the 1-tissue model were $V_b = 0.0544$ ml/ml, $K_1 = 0.252$ ml/min/ml, $k_2 = 0.104$/min and $V_T = 2.45$ ml/ml. The mean AICs of the 1-tissue and 2-tissue models were 563 and 519, respectively. Since the mean AIC of the 2-tissue model was significantly lower than that of the 1-tissue model by paired t test ($P < 0.0005$), the 2-tissue model was preferred over the 1-tissue model for describing the cerebellar TAC. The mean K_1/k_2 values of striatal regions were 9.79 (caudate) and 11.2 (putamen), and were significantly higher than those of other regions (approximately 2.0). In addition, the coefficients of variation of K_1/k_2 in striatal regions were 47.9% (caudate) and 23.5% (putamen), whereas those of other regions ranged from 10.6 to 16.8%, except for pons (26.6%) and white matter (26.5%).

Plasma-input Logan analysis was also performed to obtain the distribution volume (V_T). Typical examples of plasma-Logan plot for putamen and midbrain are shown in Fig. 5. V_T values obtained by kinetic analysis and plasma-input Logan analysis are shown in Table 1. The t^* of striatal regions ranged from 24 to 52 min. The caudate

Table 1 Mean kinetic parameters and total distribution volumes estimated by each analysis in humans ($n = 6$)

Region	2-Tissue model analysis						Graphical analysis
	V_b (ml/ml)	K_1 (ml/min/ml)	k_2 (/min)	k_3 (/min)	k_4 (/min)	V_T (ml/ml)	V_T (ml/ml)
Cerebellum	0.0318 (14.7)	0.264 (18.7)	0.128 (21.3)	0.00892 (59.0)	0.0189 (54.1)	3.08 (15.7)	2.79 (18.1)
Pons	0.0325 (28.9)	0.217 (17.8)	0.107 (39.8)	0.0213 (67.9)	0.0286 (74.3)	4.45 (46.6)	3.38 (21.9)
Temporal cortex	0.0405 (17.4)	0.211 (15.4)	0.109 (22.7)	0.0115 (55.8)	0.0151 (75.4)	4.43 (49.4)	2.96 (10.5)
Frontal cortex	0.0371 (18.0)	0.236 (16.7)	0.130 (24.0)	0.0152 (45.3)	0.0168 (36.2)	3.50 (16.7)	3.12 (17.6)
Occipital cortex	0.0239 (53.5)	0.244 (12.2)	0.126 (23.8)	0.0125 (32.0)	0.0159 (30.9)	3.59 (18.8)	3.18 (17.0)
Caudate	0.0346 (19.5)	0.252 (19.5)	0.0336 (60.6)	0.0936 (122)	0.0178 (34.7)	43.2 (25.9)	35.3 (22.9)
Thalamus	0.0299 (41.1)	0.262 (25.6)	0.153 (83.3)	0.0781 (202)	0.0409 (85.9)	3.77 (18.0)	3.49 (20.9)
Putamen	0.0394 (24.7)	0.276 (23.1)	0.0269 (47.2)	0.0441 (54.7)	0.0143 (24.6)	42.9 (21.7)	33.7 (30.8)
Midbrain	0.0366 (25.1)	0.161 (18.0)	0.0810 (36.4)	0.0441 (71.0)	0.0347 (34.3)	4.54 (20.7)	4.23 (17.9)
Parahippocampal gyrus	0.0422 (14.8)	0.160 (21.3)	0.0859 (27.9)	0.0126 (64.1)	0.0196 (65.5)	2.98 (22.9)	2.78 (22.7)
Anterior cingulate	0.0434 (16.9)	0.234 (20.6)	0.118 (20.7)	0.0137 (38.2)	0.0165 (35.8)	3.65 (14.6)	3.12 (17.4)
Parietal cortex	0.0396 (14.0)	0.248 (16.7)	0.128 (22.2)	0.0119 (38.6)	0.0140 (37.2)	3.68 (15.2)	3.15 (14.1)
White matter	0.0136 (15.9)	0.093 (24.5)	0.0821 (43.9)	0.0756 (79.4)	0.0319 (15.7)	3.78 (16.5)	3.62 (20.1)

Mean and coefficient of variation in *parentheses* are expressed as mean value and normalized SD of each parameter for six subjects

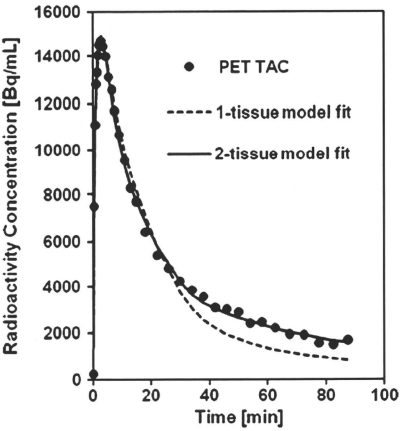

Fig. 4 Typical example of cerebellar time–activity curve and fitted model curves. *Filled circles*, *solid line* and *dashed line* represent measured time–activity curves, the 2-tissue model curve and the 1-tissue model curve, respectively. The estimated parameters for 1-tissue model fit were $V_b = 0.0521$ ml/ml, $K_1 = 0.302$ ml/min/ml and $k_2 = 0.132$/min. Those for 2-tissue model fit were $V_b = 0.0269$ ml/ml, $K_1 = 0.320$ ml/min/ml, $k_2 = 0.161$/min, $k_3 = 0.00824$/min and $k_4 = 0.0167$/min. The resultant AIC for 1-tissue model fit and 2-tissue model fit were 585 and 532, respectively

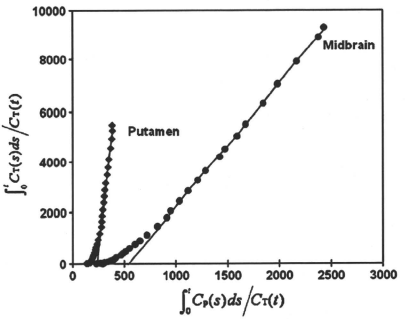

Fig. 5 Examples of plasma-Logan plot of the TACs in Fig. 3. For the putamen, t^* was 52 min, and V_T estimated with plasma-Logan analysis was 34.3 ml/ml, whereas V_T estimated with the 2-tissue compartment model was 40.8 ml/ml. For the midbrain, t^* was 24 min and V_T estimated with plasma-Logan analysis was 5.11 ml/ml, whereas V_T estimated with the 2-tissue compartment model was 4.84 ml/ml

TAC of $t^* = 24$ min was re-analyzed with fixed t^* at 52 min. The estimated V_T values were 34.2 ml/ml ($t^* = 24$ min) and 35.7 ml/ml ($t^* = 52$ min), respectively. The relative difference generated by longer t^* was about 4%. t^* of other regions ranged from 7 min (thalamus) to 32 min (occipital). Overall, V_T values obtained by plasma-input Logan analysis were lower than those by kinetic analysis (approximately, 20% underestimation).

Reference tissue model analysis (noninvasive analysis)

With the SRTM method, 5 of 60 brain TACs, except the caudate and putamen, failed to converge and were excluded from further evaluation. The relationship between *DVR* obtained by plasma-input Logan analysis and the reference tissue models is presented in Fig. 6a. The estimated *DVR* was found to be underestimated in the striatal regions showing high *DVR*. Figure 6b focused on the lower *DVR* part of Fig. 6a. In the lower *DVR* range, *DVR* values were consistent between plasma-input Logan analysis and the reference tissue model methods ($R^2 = 0.940$ for MRTMo and $R^2 = 0.607$ for SRTM, respectively). The regional *DVR*s estimated with MRTMo and SRTM in low *DVR* regions are summarized in Table 2. The time t^* of MRTMo ranged from 3.5 min (thalamus) to 26 min (pons and anterior cingulate).

Simulation study

The relationship between the estimated *DVR* by MRTMo and SRTM methods and assumed *DVR* calculated with kinetic parameters, with tracer kinetics in the reference region being described by the 2-tissue model, is shown in Fig. 7a and b. The relationship was curvilinear, similar to the result of the clinical study. Consequently, when assumed *DVR*s were 9.64 and 20.4, estimated *DVR*s were 6.91 (28.3% underestimation) and 11.2 (45.1% underestimation) by MRTMo, and 7.26 (24.7% underestimation) and 11.1 (45.6% underestimation) by SRTM, respectively. Though there was underestimation in the high *DVR* range, Fig. 7b also demonstrated the applicability of the reference tissue models in a lower *DVR* range. The time t^* of MRTMo ranged from 1.5 min to 18 min. t^* of *DVR*s over 10, corresponding to those of striatal regions, ranged from 5.5 to 13 min and were comparable to the human results. When tracer kinetics in the reference region was described by the 1-tissue model, the relationship between estimated and assumed *DVR* became almost linear for the entire *DVR* range (Fig. 7c).

The results of the simulation for the extended scan duration up to 4 h, when the reference tissue kinetics was the 2-tissue model, are shown in Fig. 7d. When the assumed *DVR*s were 9.64 and 20.4, estimated *DVR*s were 7.89 (18.1% underestimation) and 14.0 (31.4%

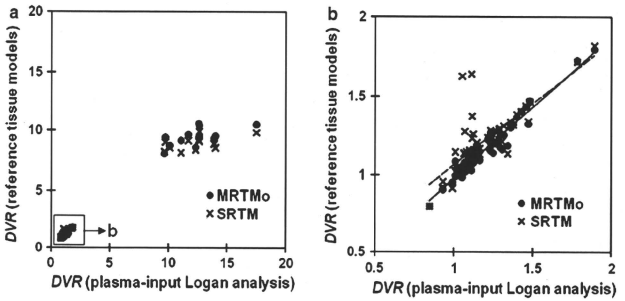

Fig. 6 **a** The relationship between *DVR* obtained by plasma-input Logan analysis and the reference tissue models. Low *DVR* range is zoomed up in (**b**). The *solid line* is the regression line for MRTMo ($y = 0.901x + 0.077$, $R^2 = 0.940$) and the *dashed line* is that for SRTM ($y = 0.785x + 0.275$, $R^2 = 0.607$)

Table 2 Distribution volume ratios obtained by graphical analysis and reference tissue models

REGION	Graphical analysis		MRTMo		SRTM	
	Mean	SD	Mean	SD	Mean	SD
Pons	1.21	0.14	1.19	0.12	1.16	0.12
Temporal cortex	1.08	0.10	1.03	0.07	1.03	0.07
Frontal cortex	1.12	0.06	1.07	0.04	1.26	0.21
Occipital cortex	1.15	0.12	1.09	0.08	1.20	0.08
Thalamus	1.25	0.13	1.27	0.11	1.25	0.11
Midbrain	1.53	0.25	1.48	0.23	1.37	0.22
Parahippocampal gyrus	0.996	0.100	0.971	0.104	1.03	0.04
Anterior cingulate	1.12	0.10	1.11	0.07	1.15	0.08
Parietal cortex	1.14	0.09	1.08	0.06	1.22	0.29
White matter	1.30	0.13	1.22	0.08	1.20	0.07

underestimation) by SRTM, and 8.65 (10.3% underestimation) and 17.5 (14.2% underestimation) by MRTMo with t^* determined within 10% discrepancy, respectively. The time t^* ranged from 1.5 to 42 min. For both reference tissue models, longer scan duration reduced the underestimation of the *DVR*s. Then, MRTMo with fixed t^* at 120 min was applied, and the estimates for assumed *DVR*s of 9.64 and 20.4 were 8.99 (6.74% underestimation) and 18.7 (8.33% underestimation), respectively. On comparing Fig. 7d with Fig. 7a, the curves became more linear and the underestimation was recovered with longer scan duration, and especially the *DVR* estimated with MRTMo with fixed t^* at 120 min. Therefore, MRTMo with delayed t^* improved the underestimation significantly.

Discussion

Regional distribution of [^{11}C]PE2I in brain was in good agreement with the known distribution of DAT in post-mortem brain [36], supporting the contention that [^{11}C]PE2I-PET imaging is an appropriate technique for visualizing DAT distribution in human brain in vivo. The ratio of radioactive concentration in the putamen to that in the cerebellum was approximately 10 at the end of the scan. These results were in agreement with a previous human PET study [22]. Estimated V_T values of striatal regions and midbrain were lower than those in previous reports [21, 22]. On the other hand, V_T of the cerebellar cortex was similar. The V_T values of the highly accumulated, small regions depend on the ROI determined and the special resolution of the PET scanner. Though the ROI delineations of the two reports were not shown, differences in the ROI delineations can be one of the reasons for such discrepancies. Another possible explanation is that since Hirvonen et al. used a high-resolution PET scanner, the partial volume effect, which causes the underestimation of V_T, may have been less marked.

Quantification using arterial input function

Although it is generally assumed that the tracer kinetics in the reference region is based on the 1-tissue model, the 2-tissue model was considered superior for describing the TAC in the cerebellum as reported previously [20, 22]. Recently, two radioactive metabolites of [^{11}C]PE2I were identified in rat brain tissue 30 min after intravenous administration of [^{11}C]PE2I [37]. One was reported to be pharmacologically active hydroxylated PE2I ([^{11}C]**1**) and the other inactive carboxyl-desmethyl-PE2I ([^{11}C]**2**). The report showed that [^{11}C]PE2I was stable in rat brain homogenates and that liver cytochrome P450 enzymes were responsible for the formation of [^{11}C]**1**, and also that [^{11}C]**2** was a metabolite of [^{11}C]**1** through alcohol and aldehyde dehydrogenases. [^{11}C]**1** is considered to enter the brain across BBB from plasma in rats, and more polar [^{11}C]**2** is considered to be transformed within the brain from [^{11}C]**1**. Nevertheless, although the metabolism and

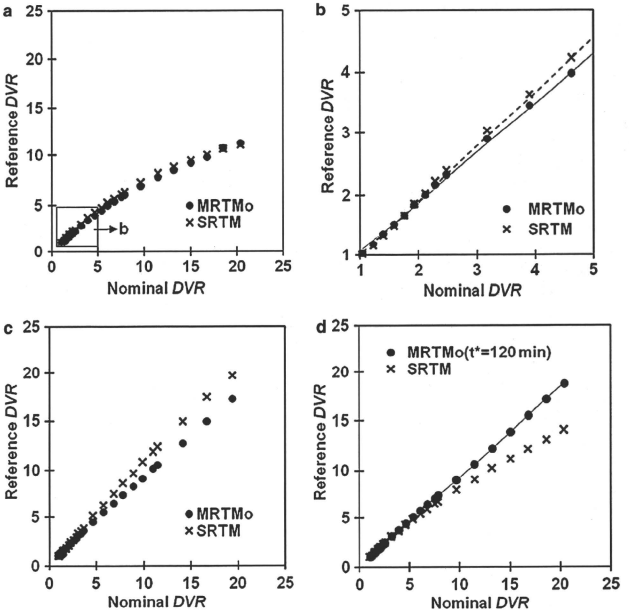

Fig. 7 **a** Simulation results of the relationship between theoretical *DVR* and estimated *DVR* by the reference tissue models when reference tissue kinetics is the 2-tissue model. **b** Zoom-up of lower *DVR* range of **a**. The *solid* and *dashed lines* are regression lines for MRTMo ($y = 0.802x + 0.268$) and SRTM ($y = 0.880x + 0.141$). **c** Simulation results of the relationship between theoretical *DVR* and estimated *DVR* by the reference tissue models when reference tissue kinetics is the 1-tissue model. **d** Simulation results of the relationship between theoretical *DVR* and estimated *DVR* when extended scan duration of 4 h was applied and the reference tissue kinetics is the 2-tissue model. The *solid line* and *dashed line* are regression lines for MRTMo with fixed t^* at 120 min ($y = 0.914x + 0.128$)

pharmacokinetics of [^{11}C]PE2I and BBB-permeability in humans may be considered different from those in rats, this cannot directly indicate that a BBB-permeable metabolite accumulated in the human brain and affected the kinetics. For the discrepancy of K_1/k_2 values between striatal regions and the other regions, the larger coefficients of variation implied that the curve fitting of these high V_T regions was somewhat unstable. On the other hand, the curve fitting using the constrained K_1/k_2 values of the cerebellum even worsened the goodness of fit for all cases (data not shown). Therefore, K_1/k_2 values of striatal regions are unlikely to be the same as that of the cerebellum.

Though various t^* values were determined across the regions in plasma-input Logan analysis, V_T values were insensitive to t^*. Therefore, uniform t^*, for example 30 min, can be applied to all regions. The estimated distribution volumes by kinetic analysis and plasma-input Logan analysis were in good agreement, although the values by the latter were systematically lower than those by the former. It was considered that 90 min was an insufficient scan time for the estimation of V_T with plasma-input Logan analysis as described in a recent study [20], in addition to the noise-induced underestimation [38]. In some cases in kinetic analysis, extremely small k_4 values (<0.01, approximately half of the averaged k_4) generated significantly large V_T values in kinetic analysis. Consequently, large discrepancies of estimated V_T values between kinetic analysis and plasma-input Logan analysis and relatively larger coefficients of variation for V_T derived by kinetic analysis than those by plasma-input Logan analysis occurred. Therefore, V_T estimated by plasma-input Logan analysis was considered more suitable to validate *DVR* estimation with the reference tissue models.

Reference tissue model methods

Underestimation of *DVR* was observed in regions with high *DVR*, i.e., the striatum for both reference tissue model methods MRTMo and SRTM as compared with plasma-input Logan analysis and kinetic analysis in the measured data as shown in Fig. 6a. Previous reports also showed underestimation of BP_{ND} in the striatum obtained with SRTM [20–22]. One of the reasons for this underestimation was considered to be the fact that the tracer kinetics in the cerebellum could be described by the 2-tissue model, while the assumption of both of the reference tissue models was

that the kinetics of the reference tissue must be described with the 1-tissue model. The results of the simulation study shown in Fig. 7a and c indicates that the TAC of the reference region underlies the underestimation of high *DVR*. Such underestimation of BP_{ND}, which is equivalent to *DVR*-1, calculated by SRTM was also reported in PET studies with [carbonyl-^{11}C]WAY-100635, a 5-HT_{1A} receptor ligand [39].

On the other hand, in the regions with low *DVR*, both the human and 90-min simulation studies showed that *DVR* estimated with the reference tissue models was well correlated with those calculated with plasma-input Logan analysis despite the violation of the assumption of the reference tissue model methods (Figs. 6b, 7b). Therefore, these methods were thought to be practically applicable under certain conditions, though the reference tissue TAC was well fitted by the 2-tissue model. Since [^{11}C]PE2I kinetics in the striatal regions is slow, we speculated that the underestimation of high *DVR* could be remedied by a longer PET data duration if physical decay of the radioisotope was allowed. The simulation extending scan duration up to 4 h showed that the underestimation could be improved by longer scan time for both methods; especially, *DVR*s estimated with MRTMo applying prolonged t^* were linearly correlated with assumed *DVR*s with a slope of 0.91 (Fig. 7d). The further improvement of the underestimation by MRTMo with prolonged t^* implies that the contribution of the latter part of the TACs was involved in the estimation of closer *DVR* to that of analysis using plasma-input function. Therefore, it is suggested that higher *DVR* estimation with the reference tissue models requires an even longer acquisition time than does the analysis using plasma-input function when reference tissue TAC is described with a 2-tissue model. However, in practice, the physical decay of ^{11}C limits the scan duration to up to 90 min.

For SRTM, it was possible to raise underestimated *DVR* by constraining lower k_2' for 90-min data. For some other established reference tissue model methods, which need predetermined k_2', *DVR* can be raised by giving smaller k_2'. Such application may remedy the underestimation of high *DVR* for 90-min data, but the validation must be carefully done.

For the estimation of lower *DVR* with the reference tissue models, 90-min scan was considered a sufficient duration. Ichise et al. [40] investigated the bias and variability of BP_{ND} estimated with several reference tissue models by simulations. They showed that MRTMo produced a variability of 5%, negative bias of 11.4% and no outliers (e.g., nonconvergent case) for a TAC with 5% noise, whereas SRTM produced 35.6% variability, 6.7% positive bias and some outliers at the same noise level when $BP_{ND} = 0.27$ ($DVR = 1.27$). In the present study, though no extreme outliner was generated, there were some nonconvergent data in the SRTM estimation results. This suggests that MRTMo reveals more stable BP_{ND} (*DVR*) but produces noise-dependent underestimation, and also that SRTM is somewhat unstable but has less deviation when BP_{ND} (*DVR*) is low. Yet, the simulation study indicated that SRTM estimates were in closer agreement with the nominal values than MRTMo estimates (Fig. 7b).

The previous study of Hirvonen et al. [21] reported excellent reproducibility in BP_{ND} of thalamus and midbrain estimated with SRTM. In the present study, both the measured and simulated data demonstrated consistency between the reference tissue models and plasma-input Logan analysis using arterial input function for 90-min data duration. Taken together, with some cautions as described above, the noninvasive approaches appear to be applicable and feasible for evaluating specific binding of [^{11}C]PE2I in lower binding regions including the midbrain and thalamus.

Conclusion

The use of SRTM and MRTMo for the estimation of *DVR*s of low-binding regions is a feasible noninvasive analysis for 90-min scan time for [^{11}C]PE2I despite the violation of the assumption of the reference tissue models. The simulation study suggested that the estimation of high *DVR* such as of striatal regions, the [^{11}C]PE2I kinetics of which is slower, needed further data duration, which is an unrealistic situation for the ^{11}C-labeled ligand. Taken together, [^{11}C]PE2I is a useful radioligand to evaluate DAT activity in lower binding regions such as the midbrain and thalamus.

Acknowledgments This study was supported by a consignment expense for the Molecular Imaging Program on "Research Base for PET Diagnosis" from the Ministry of Education, Culture, Sports, Science and Technology (MEXT), Japanese Government. The authors are thankful to Ms. Yoshiko Fukushima for organization of the clinical study and to the staff of the PET facility for their clinical assistance. We are also grateful to Dr. Masanori Ichise for his professional advice regarding the use of MRTMo, Prof. Adriaan A. Lammertsma for his kind assistance with the derivation of SRTM for *DVR* and to Dr. Mika Naganawa for constructive comments in the preparation of the manuscript.

References

1. Fowler JS, Volkow ND, Wolf AP, Dewey SL, Schlyer DJ, Macgregor RR, et al. Mapping cocaine binding sites in human and baboon brain in vivo. Synapse. 1989;4(4):371–7.
2. Hantraye P, Brownell AL, Elmaleh D, Spealman RD, Wullner U, Brownell GL, et al. Dopamine fiber detection by [^{11}C]-CFT and PET in a primate model of Parkinsonism. Neuroreport. 1992;3(3):265–8.
3. Wong DF, Yung B, Dannals RF, Shaya EK, Ravert HT, Chen CA, et al. In vivo imaging of baboon and human dopamine transporters by positron emission tomography using [11C]WIN 35, 428. Synapse. 1993;15(2):130–42.

4. Muller L, Halldin C, Farde L, Karlsson P, Hall H, Swahn CG, et al. [^{11}C] beta-CIT, a cocaine analogue. Preparation, autoradiography and preliminary PET investigations. Nucl Med Biol. 1993;20(3):249–55.
5. Halldin C, Farde L, Lundkvist C, Ginovart N, Nakashima Y, Karlsson P, et al. [^{11}C]beta-CIT-FE, a radioligand for quantitation of the dopamine transporter in the living brain using positron emission tomography. Synapse. 1996;22(4):386–90.
6. Ding YS, Fowler JS, Volkow ND, Gatley SJ, Logan J, Dewey SL, et al. Pharmacokinetics and in vivo specificity of [^{11}C]DL-threo-methylphenidate for the presynaptic dopaminergic neuron. Synapse. 1994;18(2):152–60.
7. Goodman MM, Kilts CD, Keil R, Shi B, Martarello L, Xing D, et al. 18F-labeled FECNT: a selective radioligand for PET imaging of brain dopamine transporters. Nucl Med Biol. 2000;27(1):1–12.
8. Fischman AJ, Bonab AA, Babich JW, Livni E, Alpert NM, Meltzer PC, et al. [^{11}C, ^{127}I] altropane: a highly selective ligand for PET imaging of dopamine transporter sites. Synapse. 2001;39(4):332–42.
9. Emond P, Garreau L, Chalon S, Boazi M, Caillet M, Bricard J, et al. Synthesis and ligand binding of nortropane derivatives: *N*-substituted 2beta-carbomethoxy-3beta-(4′-iodophenyl)nortropane and *N*-(3-iodoprop-(2E)-enyl)-2beta-carbomethoxy-3beta-(3′,4′-disubstituted phenyl)nortropane. New high-affinity and selective compounds for the dopamine transporter. J Med Chem. 1997;40(9):1366–72.
10. Chalon S, Hall H, Saba W, Garreau L, Dolle F, Halldin C, et al. Pharmacological characterization of (E)-*N*-(4-fluorobut-2-enyl)-2beta-carbomethoxy-3beta-(4′-tolyl)nortropane (LBT-999) as a highly promising fluorinated ligand for the dopamine transporter. J Pharmacol Exp Ther. 2006;317(1):147–52.
11. Halldin C, Erixon-Lindroth N, Pauli S, Chou YH, Okubo Y, Karlsson P, et al. [^{11}C]PE2I: a highly selective radioligand for PET examination of the dopamine transporter in monkey and human brain. Eur J Nucl Med Mol Imaging. 2003;30(9):1220–30.
12. Leroy C, Comtat C, Trebossen R, Syrota A, Martinot JL, Ribeiro MJ. Assessment of ^{11}C-PE2I binding to the neuronal dopamine transporter in humans with the high-spatial-resolution PET scanner HRRT. J Nucl Med. 2007;48(4):538–46.
13. Prunier C, Bezard E, Montharu J, Mantzarides M, Besnard JC, Baulieu JL, et al. Presymptomatic diagnosis of experimental Parkinsonism with ^{123}I-PE2I SPECT. Neuroimage. 2003;19(3):810–6.
14. Prunier C, Payoux P, Guilloteau D, Chalon S, Giraudeau B, Majorel C, et al. Quantification of dopamine transporter by ^{123}I-PE2I SPECT and the noninvasive Logan graphical method in Parkinson's disease. J Nucl Med. 2003;44(5):663–70.
15. Jucaite A, Fernell E, Halldin C, Forssberg H, Farde L. Reduced midbrain dopamine transporter binding in male adolescents with attention-deficit/hyperactivity disorder: association between striatal dopamine markers and motor hyperactivity. Biol Psychiatry. 2005;57(3):229–38.
16. Poyot T, Conde F, Gregoire MC, Frouin V, Coulon C, Fuseau C, et al. Anatomic and biochemical correlates of the dopamine transporter ligand ^{11}C-PE2I in normal and Parkinsonian primates: comparison with 6-[^{18}F]fluoro-L-dopa. J Cereb Blood Flow Metab. 2001;21(7):782–92.
17. Arakawa R, Ichimiya T, Ito H, Takano A, Okumura M, Takahashi H, et al. Increase in thalamic binding of [^{11}C]PE2I in patients with schizophrenia: a positron emission tomography study of dopamine transporter. J Psychiatr Res. 2009;43(15):1219–23.
18. Pinborg LH, Videbaek C, Svarer C, Yndgaard S, Paulson OB, Knudsen GM. Quantification of [^{123}I]PE2I binding to dopamine transporters with SPET. Eur J Nucl Med Mol Imaging. 2002;29(5):623–31.
19. Pinborg LH, Ziebell M, Frokjaer VG, de Nijs R, Svarer C, Haugbol S, et al. Quantification of ^{123}I-PE2I binding to dopamine transporter with SPECT after bolus and bolus/infusion. J Nucl Med. 2005;46(7):1119–27.
20. Delorenzo C, Kumar JD, Zanderigo F, Mann JJ, Parsey RV. Modeling considerations for in vivo quantification of the dopamine transporter using [^{11}C]PE2I and positron emission tomography. J Cereb Blood Flow Metab. 2009;29(7):1332–45.
21. Hirvonen J, Johansson J, Teras M, Oikonen V, Lumme V, Virsu P, et al. Measurement of striatal and extrastriatal dopamine transporter binding with high-resolution PET and [^{11}C]PE2I: quantitative modeling and test–retest reproducibility. J Cereb Blood Flow Metab. 2008;28(5):1059–69.
22. Jucaite A, Odano I, Olsson H, Pauli S, Halldin C, Farde L. Quantitative analyses of regional [^{11}C]PE2I binding to the dopamine transporter in the human brain: a PET study. Eur J Nucl Med Mol Imaging. 2006;33(6):657–68.
23. Lammertsma AA, Hume SP. Simplified reference tissue model for PET receptor studies. Neuroimage. 1996;4(3 Pt 1):153–8.
24. Ichise M, Ballinger JR, Golan H, Vines D, Luong A, Tsai S, et al. Noninvasive quantification of dopamine D2 receptors with iodine-123-IBF SPECT. J Nucl Med. 1996;37(3):513–20.
25. Huang SC, Barrio JR, Phelps ME. Neuroreceptor assay with positron emission tomography: equilibrium versus dynamic approaches. J Cereb Blood Flow Metab. 1986;6(5):515–21.
26. Innis RB, Cunningham VJ, Delforge J, Fujita M, Gjedde A, Gunn RN, et al. Consensus nomenclature for in vivo imaging of reversibly binding radioligands. J Cereb Blood Flow Metab. 2007;27(9):1533–9.
27. Mintum MA, Raichle ME, Kilbourn MR, Wooten GL, Welch MJ. A quantitative model for the in vivo assessment of drug binding sites with positron emission tomography. Ann Neurol. 1984;15:217–27.
28. Akaike H. A new look at the statistical model identification. IEEE Trans Automat Control. 1974;19:716–23.
29. Logan J, Fowler JS, Volkow ND, Wolf AP, Dewey SL, Schlyer DJ, et al. Graphical analysis of reversible radioligand binding from time–activity measurements applied to [*N*-^{11}C-methyl]-(−)-cocaine PET studies in human subjects. J Cereb Blood Flow Metab. 1990;10(5):740–7.
30. Hurley MJ, Mash DC, Jenner P. Markers for dopaminergic neurotransmission in the cerebellum in normal individuals and patients with Parkinson's disease examined by RT-PCR. Eur J Neurosci. 2003;18(9):2668–72.
31. Suzuki K, Sasaki M, Kubodera A. Approach to ultra high specific activity for 11C-labeled compounds. Synthesis of [11C]FLB 457 and [11C]Ro-15–4513. J Labelled Comp Radiopharm. 1999;42:S129–31.
32. Suzuki K, Inoue O, Tamate K, Mikado F. Production of 3-*N*-[^{11}C]methylspiperone with high specific activity and high radiochemical purity for PET studies: suppression of its radiolysis. Int J Rad Appl Instrum A. 1990;41(6):593–9.
33. Brix G, Zaers J, LE Adam, Bellemann ME, Ostertag H, Trojan H, et al. Performance evaluation of a whole-body PET scanner using the NEMA protocol. National Electrical Manufacturers Association. J Nucl Med. 1997;38(10):1614–23.
34. Eriksson L, Holte S, Bohm C, Kesselberg M, Hovander B. Automated blood sampling system for positron emission tomography. IEEE Trans Nucl Sci. 1988;35:703–7.
35. Friston KJ, Holmes AP, Poline JB, Grasby PJ, Williams SC, Frackowiak RS, et al. Analysis of fMRI time-series revisited. Neuroimage. 1995;2(1):45–53.
36. Hall H, Halldin C, Guilloteau D, Chalon S, Emond P, Besnard J, et al. Visualization of the dopamine transporter in the human brain postmortem with the new selective ligand [^{125}I]PE2I. Neuroimage. 1999;9(1):108–16.

37. Shetty HU, Zoghbi SS, Liow JS, Ichise M, Hong J, Musachio JL, et al. Identification and regional distribution in rat brain of radiometabolites of the dopamine transporter PET radioligand [^{11}C]PE2I. Eur J Nucl Med Mol Imaging. 2007;34(5):667–78.
38. Slifstein M, Laruelle M. Effects of statistical noise on graphic analysis of PET neuroreceptor studies. J Nucl Med. 2000;41(12): 2083–8.
39. Parsey RV, Slifstein M, Hwang DR, Abi-Dargham A, Simpson N, Mawlawi O, et al. Validation and reproducibility of measurement of 5-HT1A receptor parameters with [carbonyl-^{11}C]WAY-100635 in humans: comparison of arterial and reference tissue input functions. J Cereb Blood Flow Metab. 2000;20(7):1111–33.
40. Ichise M, Liow JS, Lu JQ, Takano A, Model K, Toyama H, et al. Linearized reference tissue parametric imaging methods: application to [^{11}C]DASB positron emission tomography studies of the serotonin transporter in human brain. J Cereb Blood Flow Metab. 2003;23(9):1096–112.

Journal of Cerebral Blood Flow & Metabolism (2010) 30, 187–195

www.jcbfm.com

Measurement error analysis for the determination of dopamine D_2 receptor occupancy using the agonist radioligand [^{11}C]MNPA

Miho Shidahara[1], Hiroshi Ito[2], Tatsui Otsuka[2], Yoko Ikoma[2,3], Ryosuke Arakawa[2], Fumitoshi Kodaka[2], Chie Seki[1], Harumasa Takano[2], Hidehiko Takahashi[2], Federico E Turkheimer[4], Yuichi Kimura[1], Iwao Kanno[1] and Tetsuya Suhara[2]

[1]*Biophysics Group, Molecular Imaging Center, National Institute of Radiological Sciences, Chiba, Japan;* [2]*Molecular Neuroimaging Group, Molecular Imaging Center, National Institute of Radiological Sciences, Chiba, Japan;* [3]*Department of Investigative Radiology, National Cardiovascular Center Research Institute, Osaka, Japan;* [4]*Department of Clinical Neuroscience, Division of Neuroscience and Mental Health, Imperial College London, London, UK*

The purpose of this study is to investigate errors in quantitative analysis for estimating dopamine D_2 receptor occupancy of antipsychotics with agonist radioligand [^{11}C]MNPA by numerical simulation, with particular attention to the validity of a quantitative approach based on the use of a reference region. Synthetic data were validated using clinical data combined with a bootstrap approach. Time–activity curves (TACs) of [^{11}C]MNPA were simulated, and the reliability of binding potential (BP_{ND}) and occupancy estimated by nonlinear least square (NLS) fitting and a simplified reference tissue model (SRTM) were investigated for various noise levels and scan durations. In the human positron emission tomography (PET) study with and without antipsychotic, risperidone, the uncertainty of BP_{ND} and occupancy estimated by SRTM was investigated using resampled TACs based on bootstrap approach with weighted residual errors of fitting. For both NLS and SRTM, it was possible to have <3% of bias in occupancy estimates of [^{11}C]MNPA by 60 mins. However, shortened scan duration degrades the quantification of very small binding potentials, especially in case of SRTM. Observations were replicated on the clinical data. Results showed that dopamine D_2 receptor occupancy by antipsychotics can be estimated precisely in region of interest analysis by SRTM with a longer than 60-min [^{11}C]MNPA PET scan duration.
Journal of Cerebral Blood Flow & Metabolism (2010) **30,** 187–195; doi:10.1038/jcbfm.2009.193; published online 16 September 2009

Keywords: positron emission tomography; dopamine D_2 receptor; occupancy; [^{11}C]MNPA; bootstrap; reference region

Introduction

The dopamine D_2 receptor exists in both high- and low-affinity states, and the state of high affinity for endogenous dopamine is defined as the functionally active form of the receptor. To determine the binding to the high-affinity state of dopamine D_2 receptors, agonist ligands have been developed (Jones *et al*, 1984; Neumeyer *et al*, 1973). It has been reported that [^{11}C]-(R)-2-CH_3O-*N*-*n*-propylnorapomorphine ([^{11}C]MNPA), one of the agonist radioligands, is more sensitive than conventional D_2 antagonist radioligands [^{11}C]raclopride to the displacement of binding by endogenous dopamine, thus proposing [^{11}C]MNPA as promising radioligand for positron emission tomography (PET) imaging of the high-affinity state of dopamine D_2 receptors in the primate brain (Seneca *et al*, 2006).

The dopamine D_2 receptor is a main therapeutic target in schizophrenia, and most antipsychotics have an antagonistic action toward dopamine D_2 receptors. Occupancy of dopamine D_2 receptors evoked by competition from antipsychotic medication can be estimated from the reduction in the observed binding potential (BP_{ND}) (Farde *et al*, 1988; Farde *et al*, 1990). Several quantitative methods have been proposed for estimating BP_{ND}, and a simplified

Correspondence: Dr H Ito, Molecular Neuroimaging Group, Molecular Imaging Center, National Institute of Radiological Sciences, Anagawa 4-9-1, Inage, Chiba 263-8555, Japan.
E-mail: hito@nirs.go.jp
Received 27 May 2009; revised 10 August 2009; accepted 11 August 2009; published online 16 September 2009

reference tissue model (SRTM) (Lammertsma and Hume, 1996) has often been used. The SRTM uses as input the time activity of a reference brain region with negligible specific binding and therefore avoids arterial blood sampling. As an occupancy study requires two PET scans, elimination of arterial blood sampling by SRTM method has practical appeal.

Otsuka *et al* (2009) showed that the SRTM method can be applied to human [^{11}C]MNPA for quantitative BP_{ND} estimation; however, a precise quantitative evaluation of the SRTM method for occupancy studies with [^{11}C]MNPA has not yet been performed. However, error analysis is important to ascertain whether the variability in occupancy with antipsychotics measured [^{11}C]MNPA is truly biological or generated by the PET measurement system. In this regard, Yokoi *et al* reported that occupancy levels of the partial agonist aripiprazole, a new antipsychotic a partial agonist for dopamine D_2 receptors without notable extrapyramidal side effects, vary widely, contrasting with the usual presence of extrapyramidal side effects at occupancy levels exceeding 80% for D_2 antagonists (Farde *et al*, 1988; Kessler, 2007; Yokoi *et al*, 2002). It is therefore of relevance to perform an error analysis of BP_{ND} estimation for PET dynamic scanning with [^{11}C]MNPA to quantify the variability induced by the measurement itself to better appreciate the biological variability that may emerge from human bioassays that use this tracer.

In this study, we simulated and evaluated errors in the quantitative analysis for the estimation of dopamine D_2 receptor occupancy when measured with [^{11}C]MNPA with particular attention to the use of SRTM. The effect of scan duration on the error of estimates was also evaluated, because shorter scan duration reduces patient's burden. Tissue kinetics where simulated using a compartmental model and, to assess model validity, we compared the results of the simulations with the errors obtained from clinical data by use of a resampling technique.

Materials and methods

Kinetics of [^{11}C]MNPA

The kinetics of [^{11}C]MNPA in the brain is based on the two-tissue three-compartment model as follows:

$$\begin{aligned}\frac{dC_{ND}(t)}{dt} &= K_1 C_P(t) - (k_2 + k_3)C_{ND}(t) + k_4 C_S(t)\\ \frac{dC_S(t)}{dt} &= k_3 C_{ND}(t) - k_4 C_S(t)\\ C_T(t) &= C_{ND}(t) + C_S(t)\end{aligned} \quad (1)$$

where C_P [Bq/mL] is the radioactivity concentration of unchanged radioligand in plasma (arterial input function), C_{ND} [Bq/cm^3] is the radioactivity concentration of nondisplaceable radioligand in brain, including nonspecifically bound and free radioligand, and C_S [Bq/cm^3] is the radioactivity concentration of radioligand specifically bound to receptors. The rate constants K_1 [mL/cm^3/min] and k_2 [min^{-1}] represent the influx and efflux rates for radioligand diffusion through the blood–brain barrier. The rate constants k_3 [min^{-1}] and k_4 [min^{-1}] represent the radioligand transfers between the compartments for nondisplaceable and specifically bound radioligand. C_T [Bq/cm^3] is the radioactivity concentration in a brain region measured by PET.

Estimation of receptor occupancy

Nonlinear least squares fitting for BP_{ND}: K_1, k_2, k_3, and k_4 values in Equation (1) can be determined by nonlinear least squares (NLS) fitting of the time–activity curve (TAC) in the target region. The cerebellum is regarded as a reference region because this brain structure has negligible D_2 dopamine receptor density (Otsuka *et al*, 2009; Seneca *et al*, 2008; Tokunaga *et al*, 2009). K_1^r and k_2^r values in the cerebellum were also determined by NLS using the one-tissue compartment model without the specific binding compartment. The BP_{ND} can be expressed using the reference region as:

$$BP_{ND} = \frac{(K_1/k_2)(k_3/k_4 + 1)}{(K_1^r/k_2^r)} - 1 \quad (2)$$

where $(K_1/k_2)(k_3/k_4 + 1)$ is the total distribution volume of the target region and (K_1^r/k_2^r) is that of the cerebellum. In this study, the calculation of BP_{ND} in Equation (2) was regarded as the standard method for BP_{ND} estimation (Otsuka *et al*, 2009). It should be noted that to improve the stability of the NLS fitting for target regions, the K_1/k_2 ratio for the target region was assumed to be the value in the cerebellum (K_1^r/k_2^r) as obtained by NLS using the one-tissue compartment model, meaning that, as a result, BP_{ND} in Equation (2) is equivalent to k_3/k_4 in this study.

Simplified reference tissue model for BP_{ND}: The SRTM yields the binding potential value by eliminating the arterial input function, C_P, arithmetically from model equations by using a TAC from a reference region where specific bindings are negligible, under the assumptions that the distribution volume of the nondisplaceable compartment was equal in the target and reference regions, and that a target region can be described with the one-tissue compartment model shown in Equation (3) (Lammertsma and Hume, 1996).

$$\begin{aligned}C_T(t) &= R_1 \cdot C_R(t) + \left(k_2 - \frac{R_1 k_2}{1 + BP_{ND}}\right) \cdot e^{\left(\frac{k_2}{1+BP_{ND}}t\right)} \otimes C_R(t)\\ R_1 &= K_1/K_1^r\end{aligned} \quad (3)$$

where C_T and C_R are the radioactivity concentrations in the target and reference regions, respectively. The SRTM estimates three parameters, the delivery ratio of the target region to reference region (R_1), the clearance rate constant of the target region (k_2), and binding potential, referred to as BP_{ND} by nonlinear least squares.

Receptor occupancy: Receptor occupancy is calculated from BP_{ND} of two scans, with and without antipsychotics, as follows:

$$Occupancy\ (\%) = 100 \cdot (BP_{control} - BP_{drug})/BP_{control} \quad (4)$$

where $BP_{control}$ represents the BP_{ND} value derived from a scan without drug and BP_{drug} represents that from a scan with drug (Farde *et al*, 1988).

Simulation study

To evaluate the dependency of the noise level and scan duration for the estimated BP_{ND} and occupancy, we performed the following simulations. Both NLS and SRTM procedures were performed using in-house software written in the C program with downhill simplex algorithm (Nelder and Mead, 1965) without weighting and without constraints for the range of estimated parameters.

Time–activity curves for [^{11}C]MNPA: A dynamic tracer concentration for [^{11}C]MNPA was derived from the kinetic parameters listed in Table 1 with a dynamic frame (20 secs × 9, 1 min × 5, 2 mins × 4, 4 mins × 11, 5 mins × 6, total 90 mins) and a measured arterial input function (10 secs × 12, 30 secs × 2, 60 secs × 7, 120 secs × 1, 180 secs × 1, 300 secs × 3, 600 secs × 6, total 90 mins) of a single subject obtained by Otsuka *et al* (2009). These K_1, k_2, and k_4 were estimated based on the two-tissue three-compartment model using NLS fitting of region of interests (ROIs) in the putamen at baseline (the number of subjects (n) = 10) (Otsuka *et al*, 2009). Furthermore, three k_3 values, 0.015, 0.075, and 0.15, were arbitrarily chosen to investigate the occupancy of antipsychotics with [^{11}C]MNPA. During a loading study with a drug, the observed binding potential (BP_{ND}) is reduced mainly due to the suppression of the radioligand transfers from the compartments for nondisplaceable to specifically bound radioligand, k_3. Therefore, we varied k_3 values while covering the practical range of occupancy from a likely level at 50% to the extreme scenario of a 90% occupancy. A measured arterial plasma input function of a single subject according to human PET imaging protocols and noise-free simulated TACs (three target curves and a reference) are shown in Figure 1A and B.

Noise was generated with random generator based on Gaussian distribution and added to the decay-corrected target TACs. The noise ratio for each time frame was determined (Ikoma *et al*, 2008) according to the collected total count given by

$$NOISE_i(\%) = \left(\sqrt{N_i}/N_i\right) \cdot 100$$
$$N_i = \int_{t_i-\frac{\Delta t_i}{2}}^{t_i+\frac{\Delta t_i}{2}} C_T(t) \cdot e^{-\lambda t} dt \cdot F \quad (5)$$

where i is the frame number, C_T is the decay-corrected tissue radioactivity concentration derived from the k-values and the input function, t_i is the midpoint time of the i-th frame, Δt_i is the data collection time, λ is the radioisotope decay constant, and F is a scaling factor representing the sensitivity of the measurement system and is introduced here for adjusting the noise level.

Noise level dependency: Target TACs of [^{11}C]MNPA with several noise levels were generated to investigate the bias and variation of parameter estimates caused by the statistical noise for NLS and SRTM. The bias and variation were calculated as %bias of estimated BP_{ND} against the true BP_{ND} value and coefficient of variance (COV) by the mean and s.d. of the estimates excluding the outliers, respectively.

In this simulation study, the noise level for dynamic data was expressed as the mean of percentage noise described in Equation (5) from 1 to 90 mins, and it was chosen so that the mean of percentage noise would be 1%, 3%, 5%, 7%, and 10%, with 500 noisy data sets being generated for each. An example of noise-added simulated TAC with $BP_{ND} = 0.417$ is shown in Figure 1C.

In these noise-added TACs, each kinetic parameter including BP_{ND} was estimated by NLS and SRTM with a noise-free reference TAC. For both NLS and SRTM, initial parameters varied by ±25% from the true value (Ichise *et al*, 2003; Ikoma *et al*, 2008), and parameter estimates were considered invalid outliers if estimated parameters were negative or more than three times the true value (Ichise *et al*, 2003; Ikoma *et al*, 2008). Occupancy was also calculated from Equation (4) by using estimated BP_{ND} with assumed $k_3 = 0.15$ as $BP_{control}$ and with assumed $k_3 = 0.015$ or 0.075 as BP_{drug}.

Scan duration: The effect of scan duration on BP_{ND} and occupancy estimates was investigated for both NLS and SRTM methods. In the 90-min simulated TACs of 3% noise level corresponding to the noise level of human ROI analysis, the duration of the scan used for the parameter estimation was progressively reduced from 90 to 32 mins (32, 44, 60, 75, and 90 mins) for [^{11}C]MNPA.

Table 1 Kinetic parameters for the simulation study of [^{11}C]MNPA

	K_1	k_2	k_3	k_4	BP_{ND}	*Occup. (%)*
Target regions	0.44	0.067	0.015	0.18	0.0833	90
			0.075		0.417	50
			0.15		0.833	—
Reference region	0.44	0.067	—	—	—	—

Human study

Subjects and positron emission tomography procedure: [^{11}C]MNPA PET studies were performed before and after antipsychotic drug administration of risperidone (0.5 and 2.0 mg) on separate days for each two healthy male volunteers (20 to 21 y.o.). Scan start time after antipsychotic administration was 4 h. The study was approved by the ethics and radiation safety committees of the National

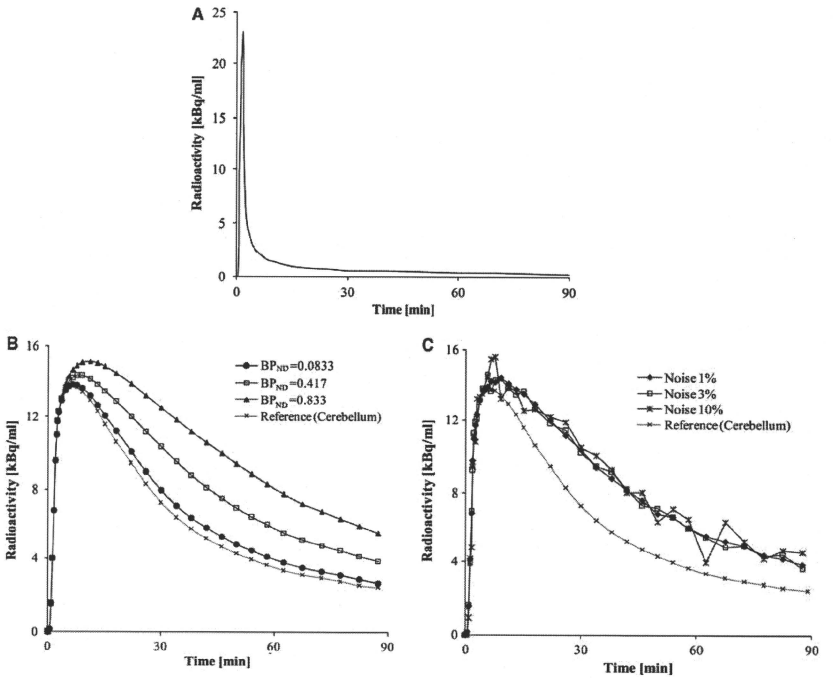

Figure 1 (**A**) Metabolite-corrected plasma input function of a single normal subject for simulation study. (**B**) Noise-free simulated TACs of three BP_{ND} values and reference TAC. (**C**) Noise-added TACs in the case of $BP_{ND} = 0.417$.

Institute of Radiological Sciences, Chiba, Japan. Written informed consent was obtained from each subject.

The PET acquisitions were performed on the ECAT EXACT HR+ (CTI-Siemens, Knoxville, TN, USA). A 10-min transmission scan with 3-rod source of ^{68}Ge–^{68}Ga was performed. Dynamic PET scans of [^{11}C]MNPA were performed for 90 mins in three-dimensional mode with a bolus injection of 208.0 to 234.0 MBq. Frame intervals were the same as this simulation study. The specific radioactivity was 245.1 to 313.8 GBq/μmol at the time of injection. Arterial blood sampling was not performed. All emission data were reconstructed by filtered-back projection using a Hanning filter with a cut-off frequency of 0.4.

Data analysis: The summed PET images for all frames were coregistered to individual MR images, and ROIs were drawn manually over the putamen, caudate, and cerebellum. Especially, R_1, k_2, and BP_{ND} in the putamen were estimated by SRTM using the cerebellum as reference region.

Human data were used to check model validity for the simulation studies. Given that an occupancy is measured only once (two scans for subject) and that repetitive measurements are not usually available, the reliability of parameter estimates can be evaluated by a bootstrap approach with weighted residual errors of fitting as published earlier (Rosso *et al*, 2009; Turkheimer *et al*, 1998). For each ROI in each individual subject data, 500 replication TACs were generated using bootstrap approach, and then parameters were estimated by SRTM and the COV of these 500 estimates was calculated to produce an accurate estimate of the statistical variability of the parameters. The weighted residual, ξ, using model-predicted tissue TAC, C_T, and the measured tissue TAC, X, were calculated as follows;

$$\xi_i = (X(t_i) - C_T(t_i)) \cdot \sqrt{N_i}$$
$$N_i = \int_{t_i - \frac{\Delta t_i}{2}}^{t_i + \frac{\Delta t_i}{2}} C_T(t) \cdot e^{-\lambda t} dt \qquad (6)$$

Then the residuals, $\{\xi_i\}$ $(i = 1, \ldots, k)$, were randomly resampled with substitution into a new set of the residuals

$\{\xi_i^*\}$. As an example with $k=5$, $[\xi_2, \xi_2, \xi_3, \xi_4, \xi_5]$ were randomly selected $[\xi_5, \xi_1, \xi_4, \xi_1, \xi_3]$ as a new residual set $[\xi_1^*, \xi_2^*, \xi_3^*, \xi_4^*, \xi_5^*]$. The bootstrapped residuals were used to generate a new data X^* defined as,

$$X^*(t_i) = C_T(t_i) + \frac{\xi_i^*}{\sqrt{N_i}} \quad (7)$$

In keeping with the simulation study, the relationship between the scan duration and COV of estimates and between the scan duration and bias was investigated by shortening the interval of fitting of the bootstrap replication TACs from 90 to 32 mins. The bias of BP_{ND} and occupancy was defined as the difference between the mean of these calculated for each truncated fitting interval and that of the 90 mins. Parameter estimates based on bootstrap approach were considered invalid outliers if estimates from X^* were negative or more than three times that of the 90 mins.

Results

Simulation study

Noise level dependency: In the NLS method, the bias of BP_{ND} was small especially at a low noise level. However, COV of BP_{ND} became larger as the noise level increased (Figure 2A). In the SRTM method, the bias of BP_{ND} was observed even though TACs were free from noise and both the bias and COV of BP_{ND} became larger as the noise increased, which is typical in the case of small BP_{ND} (Figure 2B). For both NLS and SRTM methods, these bias and COV values of occupancy were smaller compared with BP_{ND}. The tendency that COV with 90% occupancy was smaller compared with that with 50% occupancy was a common observation for NLS and SRTM.

Scan duration: The relationship between the reliability of BP_{ND} and occupancy estimates and the scan duration was investigated as shown in Figure 3. The bias of BP_{ND} and occupancy estimated by NLS was small despite short scan durations (Figure 3A); however, more than 10% outliers was caused with $BP_{ND}=0.0833$ at 32, 44, 60, 75, and 90 mins (Table 2). As scanning time became shorter, BP_{ND} for all three conditions was overestimated by SRTM (Figure 3B) and its bias magnitude was larger than that of NLS. More than 10% outliers was seen with $BP_{ND}=0.0833$ at 32 and 44 mins, $BP_{ND}=0.417$ at 32 mins and 0.833 at 32 mins. Bias was under 3% at a 3% noise level with occupancy estimates by SRTM method with scan duration longer than 60 mins (Figure 3B).

Human study

Time–activity curves: As shown in Figure 4, the shape of the TACs was similar between before and after antipsychotic administration in the cerebellum, whereas the accumulation of radioactivity in the postantipsychotic scan decreased at late times in other regions. In Figure 4A and B, estimated BP_{ND} in putamen of a subject before and after administration of Risperidone 2 mg were 0.968 and 0.437, then its occupancy resulted in 54.8%. For the other subject shown in Figure 4C and D, estimated BP_{ND} in putamen of a subject before and after administration

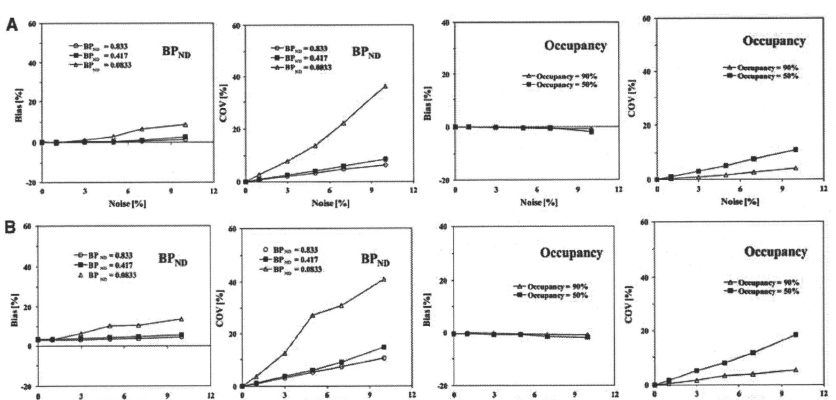

Figure 2 Noise level dependency. (**A**) Bias and COV of BP_{ND} and occupancy estimated by NLS ($K_1/k_2 = 6.6$ fixed), (**B**) estimated by SRTM.

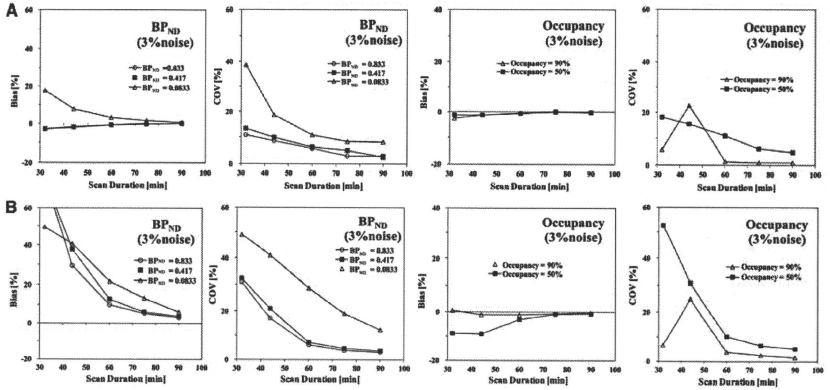

Figure 3 Scan duration dependency of bias and COV of BP_{ND} and occupancy at a 3% noise level estimated by (**A**) NLS and (**B**) SRTM methods.

Table 2 Scan duration dependency on the percentages of outliers of BP_{ND} at 3% noise level estimated by NLS and SRTM

	BP_{ND}	*Scan duration (min)*				
		32	*44*	*60*	*75*	*90*
NLS	0.0833	27.4	22.8	22.6	12.8	10.8
	0.417	5.8	3.4	1.4	2.6	1.2
	0.833	3.8	1.8	0.2	0	0
SRTM	0.0833	40.4	19.8	3.4	0.2	0
	0.417	29.2	0.6	0	0	0
	0.833	26.0	0.2	0	0	0

NLS, nonlinear least square; SRTM, simplified reference tissue model.

of Risperidone 0.5 mg were 0.866 and 0.496, then its occupancy resulted in 42.7%.

Scan duration: On the basis of the bootstrap approach, the relationship between the reliability of BP_{ND} and occupancy estimates and the scan duration was investigated as shown in Figure 5.

As scanning time became shorter, BP_{ND} in both before and after antipsychotics administration for two volunteers was overestimated. However, the bias of occupancy was small despite short scan durations. The COVs of both BP_{ND} and occupancy also became larger with shorter scan durations. These observations are consistent with the simulation results especially in the case of occupancy shown in Figure 3B, even though a small difference of magnitude of bias in BP_{ND} was still observed.

Discussion

In this study, we evaluated the effect of noise and scan duration of dynamic PET [^{11}C]MNPA studies on the BP_{ND} estimates obtained with NLS and SRTM for a range of BP_{ND} values, a range that is likely to be encountered in occupancy studies with antipsychotic medication. Error analysis was performed using artificial datasets. The validity of the simulations was assessed by using the bootstrap on a small cohort of human data to calculate 'real variances' that resulted in good agreement with those obtained from the artificial datasets.

Reliability of estimated parameters

In the case of NLS, the larger number of parameters introduced instability and, even though we introduced a fixed K_1/k_2 ratio, the variability of BP_{ND} was still significant as shown by the percentage of outliers by NLS (Table 2). K_1/k_2 for both target and reference regions were same in this simulation study; however, in clinical situation, sometimes K_1/k_2 values may vary from regions to regions (Ginovart *et al*, 2007) and these difference may introduce errors in BP_{ND} when the ratio K_1/k_2 is fixed.

The SRTM provided reliable estimates although variability increased for low BP_{ND} values even with favorable noise levels (Gunn *et al*, 1997; Ikoma *et al*, 2008). As shown in Figure 2B, both bias and COV with small $BP_{ND} = 0.0833$ were larger than those with $BP_{ND} = 0.417$ or 0.833. The small bias of BP_{ND} estimates in noise-free TACs (Figure 2B) may originate from the two-tissue model of the target

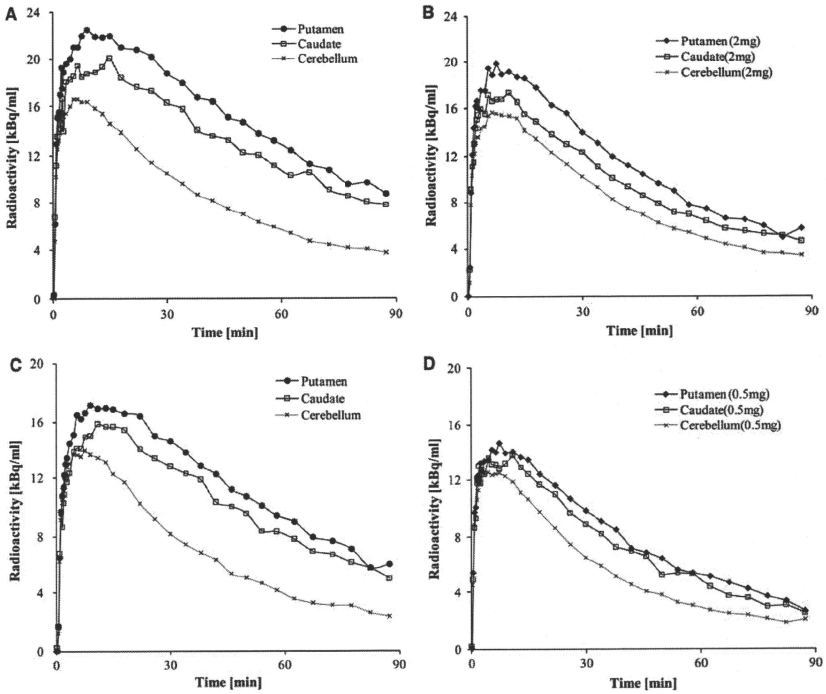

Figure 4 TACs for a single subject with baseline (**A**), and 2 mg administration of Risperidone (**B**), TAC for the other subject with baseline (**C**), and 0.5 mg administration of Risperidone (**D**). ROIs were drawn on putamen, caudate, and cerebellum.

tissue. In the SRTM method, even when the one-tissue model for target tissue is not appropriate, the apparent rate constant ($=k_2/(1+BP_{ND})$ in Equation (3) could be used to fit the curves well and bias in BP_{ND} is negligible (Wu and Carson, 2002). In this study, as shown in Figure 2B, the bias of BP_{ND} was small and the error propagation of biased BP_{ND} to occupancy in the SRTM method was also small. Errors of both estimated BP_{ND} and occupancy by SRTM were small at a low noise level, indicating that ROI analysis of SRTM will be useful for a quantified BP_{ND} and occupancy study with [^{11}C]MNPA.

In the simulation study, the reference TAC was assumed as noise free; however, noise may affect the reference TAC depending on the size of ROI (Ogden and Tarpey, 2006). For SRTM, the use of a 1% noise on the reference TAC increased %COV of the BP_{ND} estimates for the target regions (where noise was 3%) by 20% to 30%. However, the noise in the reference TAC did not change the profile of BP_{ND} %COV in the target TAC according to scan duration nor changed the biases in the estimated occupancies that remained similar.

Effects of scan duration

In the simulation study, a 60-min scan duration gave unbiased and reliable BP_{ND} and occupancy estimates by NLS with [^{11}C]MNPA both at baseline and with drug load (Figure 3A). Conversely, the results of SRTM method showed that at least 60-min scan duration would be required for the quantification of occupancy; bias was under 3% at a 3% noise level with scan duration longer than 60 mins (Figure 3B). Shorter scan duration caused larger bias of BP_{ND} estimated by SRTM. Note that the sampling rate of the reference input function is inherently lower than

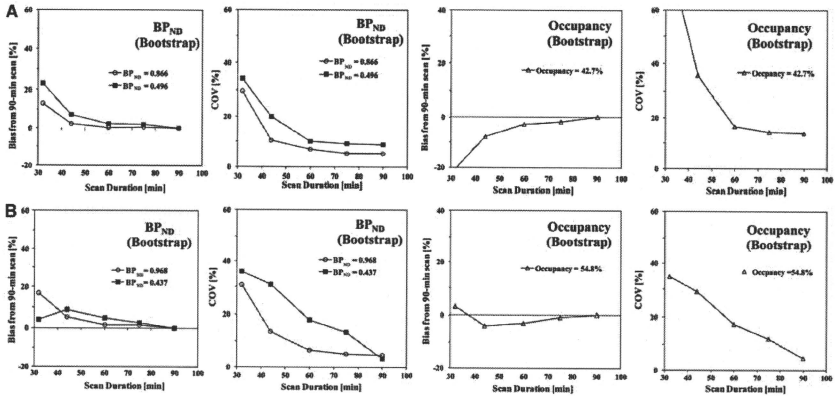

Figure 5 Scan duration dependency of bias and COV of BP_{ND} and occupancy in the putamen estimated by SRTM method for a single subject with 0.5 mg administration (**A**) and the other subject with 2 mg administration (**B**).

the one of the plasma input function and this may introduce errors with SRTM although in this instance, kinetics in tissue are not particularly fast.

The use of the bootstrap approach on clinical data validated most of the observations obtained from simulations for the SRTM method, such as the overestimation of BP_{ND} and underestimation of occupancy at shorter scan durations. It is important to remark that the variability considered here is the one associated with the measurement error only. Further variability of biological origin (between subjects and/or associated with age, gender, etc. (Inoue *et al*, 2001; Kaasinen *et al*, 2001)) should be taken into account and possibly controlled at the design stage.

We can therefore conclude that, for both NLS and SRTM methods, reliable and unbiased occupancy estimates of [^{11}C]MNPA could be obtained by 60 mins, with COV of 50% occupancy remaining at 11.0% and 10.1%, respectively (Figure 3). In the case of lower occupancy than 50%, COV at 60-min scan duration may be >11% but no bias should be expected.

Conclusion

The effects of bias, variance, and scan duration in PET quantitative analysis of dopamine D_2 receptor occupancy using [^{11}C]MNPA were evaluated in a simulation study and validated using a bootstrap approach on clinical data. The results suggest that a reference approach with SRTM applied to ROI data with a scan duration of at least 60-mins PET scan duration represent a valid bioassay for the task.

Acknowledgements

This study was supported in part by Grants-in-Aid for Young Scientists (B) (No. 19700395) and by a consignment expense for the Molecular Imaging Program on 'Research Base for PET Diagnosis' from the Ministry of Education, Culture, Sports, Science and Technology (MEXT), Japanese Government and by the Royal Society, International Project Grant no. JP0871550, UK. We thank Dr Hiroshi Watabe for his valuable advice.

Conflict of interest

The authors declare no conflict of interest.

References

Farde L, Wiesel FA, Halldin C, Sedvall G (1988) Central D2-dopamine receptor occupancy in schizophrenic patients treated with antipsychotic drugs. *Arch Gen Psychiatry* 45:71–6

Farde L, Wiesel FA, Stone-Elander S, Halldin C, Nordstrom AL, Hall H, Sedvall G (1990) D2 dopamine receptors in neuroleptic-naive schizophrenic patients. A positron emission tomography study with [11C]raclopride. *Arch Gen Psychiatry* 47:213–9

Ginovart N, Willeit M, Rusjan P, Graff A, Bloomfield PM, Houle S, Kapur S, Wilson AA (2007) Positron emission tomography quantification of [11C]-(+)-PHNO binding in the human brain. *J Cereb Blood Flow Metab* 27:857–71

Gunn RN, Lammertsma AA, Hume SP, Cunningham VJ (1997) Parametric imaging of ligand-receptor binding in PET using a simplified reference region model. *Neuroimage* 6:279–87

Ichise M, Liow JS, Lu JQ, Takano A, Model K, Toyama H, Suhara T, Suzuki K, Innis RB, Carson RE (2003) Linearized reference tissue parametric imaging methods: application to [11C]DASB positron emission tomography studies of the serotonin transporter in human brain. *J Cereb Blood Flow Metab* 23:1096–112

Ikoma Y, Ito H, Arakawa R, Okumura M, Seki C, Shidahara M, Takahashi H, Kimura Y, Kanno I, Suhara T (2008) Error analysis for PET measurement of dopamine D2 receptor occupancy by antipsychotics with [11C]raclopride and [11C]FLB 457. *Neuroimage* 42:1285–94

Inoue M, Suhara T, Sudo Y, Okubo Y, Yasuno F, Kishimoto T, Yoshikawa K, Tanada S (2001) Age-related reduction of extrastriatal dopamine D2 receptor measured by PET. *Life Sci* 69:1079–84

Jones JH, Anderson PS, Baldwin JJ, Clineschmidt BV, McClure DE, Lundell GF, Randall WC, Martin GE, Williams M, Hirshfield JM *et al* (1984) Synthesis of 4-substituted 2H-naphth[1,2-b]-1,4-oxazines, a new class of dopamine agonists. *J Med Chem* 27:1607–13

Kaasinen V, Nagren K, Hietala J, Farde L, Rinne JO (2001) Sex differences in extrastriatal dopamine d(2)-like receptors in the human brain. *Am J Psychiatry* 158:308–11

Kessler RM (2007) Aripiprazole: what is the role of dopamine D(2) receptor partial agonism? *Am J Psychiatry* 164:1310–2

Lammertsma AA, Hume SP (1996) Simplified reference tissue model for PET receptor studies. *Neuroimage* 4:153–8

Nelder JA, Mead R (1965) A simplex method for function minimization. *Comput J* 7:308–13

Neumeyer JL, Neustadt BR, Oh KH, Weinhardt KK, Boyce CB, Rosenberg FJ, Teiger DG (1973) Aporphines. 8. Total synthesis and pharmacological evaluation of (plus or minus)-apomorphine, (plus or minus)-apocodeine, (plus or minus)-N-n-propylnorapomorphine, and (plus or minus)-N-n-propylnorapocodeine. *J Med Chem* 16:1223–8

Ogden RT, Tarpey T (2006) Estimation in regression models with externally estimated parameters. *Biostatistics* 7:115–29

Otsuka T, Ito H, Halldin C, Takahashi H, Takano H, Arakawa R, Okumura M, Kodaka F, Miyoshi M, Sekine M, Seki C, Nakao R, Suzuki K, Finnema SJ, Hirayama Y, Suhara T, Farde L (2009) Quantitative PET analysis of the dopamine D2 receptor agonist radioligand 11C-(R)-2-CH3O-N-n-propylnorapomorphine in the human brain. *J Nucl Med* 50:703–10

Rosso L, Brock CS, Gallo JM, Saleem A, Price PM, Turkheimer FE, Aboagye EO (2009) A new model for prediction of drug distribution in tumor and normal tissues: pharmacokinetics of temozolomide in glioma patients. *Cancer Res* 69:120–7

Seneca N, Finnema SJ, Farde L, Gulyas B, Wikstrom HV, Halldin C, Innis RB (2006) Effect of amphetamine on dopamine D2 receptor binding in nonhuman primate brain: a comparison of the agonist radioligand [^{11}C]MNPA and antagonist [^{11}C]raclopride. *Synapse* 59:260–9

Seneca N, Skinbjerg M, Zoghbi SS, Liow JS, Gladding RL, Hong J, Kannan P, Tuan E, Sibley DR, Halldin C, Pike VW, Innis RB (2008) Kinetic brain analysis and whole-body imaging in monkey of [^{11}C]MNPA: a dopamine agonist radioligand. *Synapse* 62:700–9

Tokunaga M, Seneca N, Shin RM, Maeda J, Obayashi S, Okauchi T, Nagai Y, Zhang MR, Nakao R, Ito H, Innis RB, Halldin C, Suzuki K, Higuchi M, Suhara T (2009) Neuroimaging and physiological evidence for involvement of glutamatergic transmission in regulation of the striatal dopaminergic system. *J Neurosci* 29: 1887–96

Turkheimer F, Sokoloff L, Bertoldo A, Lucignani G, Reivich M, Jaggi JL, Schmidt K (1998) Estimation of component and parameter distributions in spectral analysis. *J Cereb Blood Flow Metab* 18:1211–22

Wu Y, Carson RE (2002) Noise reduction in the simplified reference tissue model for neuroreceptor functional imaging. *J Cereb Blood Flow Metab* 22:1440–52

Yokoi F, Grunder G, Biziere K, Stephane M, Dogan AS, Dannals RF, Ravert H, Suri A, Bramer S, Wong DF (2002) Dopamine D2 and D3 receptor occupancy in normal humans treated with the antipsychotic drug aripiprazole (OPC 14597): a study using positron emission tomography and [11C]raclopride. *Neuropsychopharmacology* 27:248–59